Available online at www.sciencedirect.com
SCIENCE DIRECT®
Tectonophysics 370 (2003) 177–191
TECTONOPHYSICS
www.elsevier.com/locate/tecto

Permeability of the rocks from the Kola superdeep borehole at high temperature and pressure: implication to fluid dynamics in the continental crust

A.V. Zharikov[a,*], V.M. Vitovtova[b], V.M. Shmonov[b], A.A. Grafchikov[b]

[a] *Institute of Geology of Ore Deposits, Petrography, Mineralogy and Geochemistry of the Russian Academy of Sciences, Staromonetny per., 35, 109017, Moscow, Russia*
[b] *Institute of Experimental Mineralogy of the Russian Academy of Sciences, 142432, Chernogolovka, Moscow, Russia*

Accepted 31 March 2003

Abstract

Permeability of the samples collected from the surface and from the depths of 8–11 km in the Kola SG-3 and from the depth of 3.8 in the KTB boreholes was studied at temperatures up to 600 °C and pressures up to 150 MPa. These PT correspond to in situ conditions of the deep parts of the superdeep boreholes and to the conditions of progressive and regressive metamorphism of the Kola series rocks. The experiments were carried out with fluid filtration parallel and normal to rock foliation and parallel to core axis. The temperature–permeability trend behavior depends on effective pressure and depth of sample collection. At low effective pressure, a temperature increase leads first to a permeability decrease and then to its increase. At higher effective pressure, inversions appear on all the temperature trends of the samples collected from great depths. In contrast, permeability of the samples selected at shallow depth (3.8 km) and on the surface decreases within the entire temperature range. As a rule, with flow parallel to foliation, the values of permeability are higher than with flow normal to foliation. The results of microstructure studies allow to conclude that microcrack initiation and closure, due to a competitive influence of temperature and pressure cause such permeability behavior. In the samples, there are two families of microcracks: with low aspect ratio and those with high aspect ratio. Their effect on rock permeability changes with temperature. On sample heating, the low aspect ratio microcracks close and, on the contrary, high aspect ratio ones open. The total effect is expressed by minima in the temperature–permeability trends. Permeability anisotropy increases with temperature, reaches a maximum at 200 °C and then decreases. Sample permeability decreases with different gradients at simultaneous increase of temperature and pressure, simulating in situ depth increase. Hence, the deep seat rocks can vary greatly in permeability and against the common background of permeability decrease with depth, local deep aquifers may occur. At PT of progressive metamorphism the permeability values were high enough to permit the fluid flow to penetrate the whole volume of rock massif. At PT of regressive metamorphism, the permeability values were a few decimal orders lower, so fluid flow could be concentrated in large disjunctive zones only.

Keywords: Kola and KTB superdeep boreholes; Core and surface samples; High temperature and pressure; Permeability; Anisotropy; Continental crust

* Corresponding author. Fax: +7-095-230-2179.
E-mail addresses: vil@igem.ru (A.V. Zharikov), shmonov@iem.ac.ru (V.M. Shmonov).

0040-1951/03/$ - see front matter © 2003 Elsevier B.V. All rights reserved.
doi:10.1016/S0040-1951(03)00185-9

1. Introduction

The studies of the Kola SG-3 (Russia) and KTB (Germany) superdeep boreholes have revealed a presence of water fluids at a depth previously considered as unreachable for them (Kozlovsky, 1987; Huenges et al., 1997). Rock permeability is a critical factor, as it controls fluid transport within the Earth's crust. The main difficulty arises from the present impossibility of measuring deep rock permeability in situ directly using remote methods. However, rock permeability data can be obtained in the laboratory on appropriate samples. The results of the porosity and permeability measurements carried out on core samples from SG-3 at room temperature and atmospheric pressure showed an increase of their values with depth (Kozlovsky, 1987). However, it is not clear if this trend is related to the true in situ rock properties or is caused by the effect of the technogenic microcracks that appeared when the samples were cored and lifted to the surface (Gorbatzevich and Medvedev, 1986; Wolter and Berckhemer, 1989). Hence, we collected the samples from the surface and from different depths in the Kola and KTB boreholes. We carried out an experimental study at temperatures up to 600 °C and pressures up to 150 MPa. These PT correspond to in situ conditions

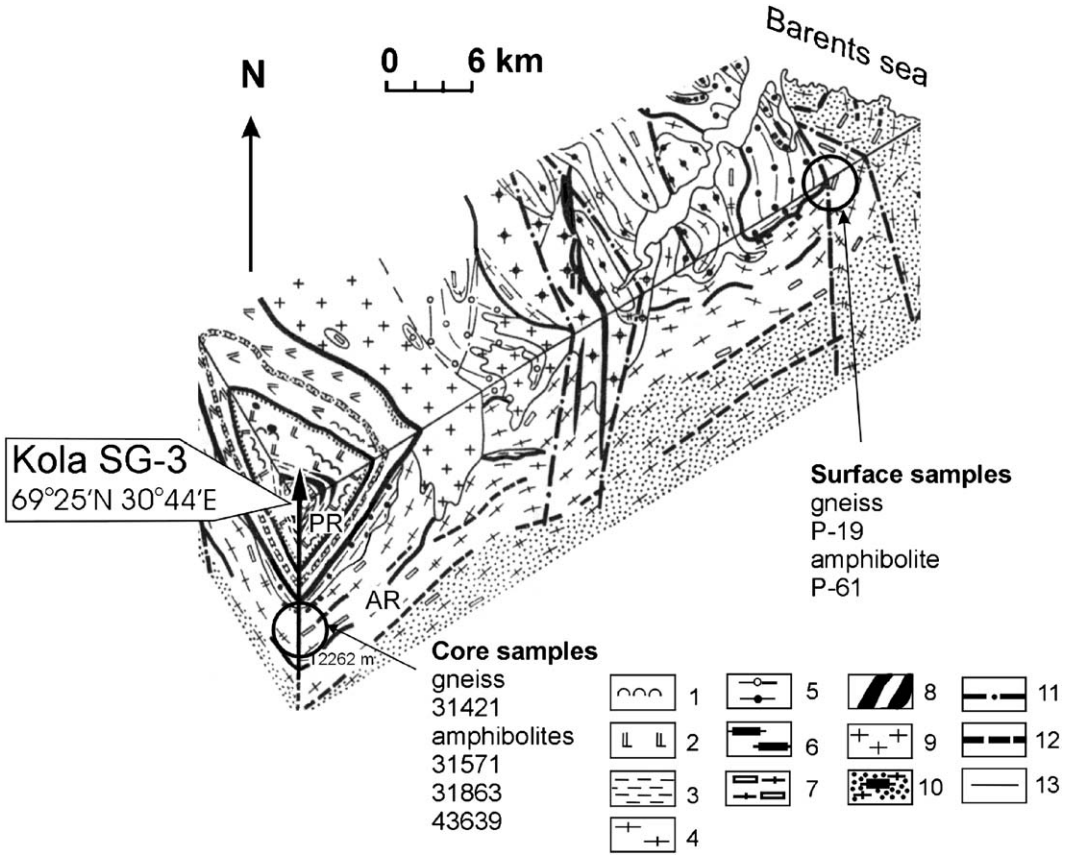

Fig. 1. Three-dimensional model of the Kola superdeep borehole area. Modified after Kozlovsky (1987). Legend: tuffs and sedimentary tufogenic rocks of different composition; metadiabases and green schists; carbonaceous phyllites, tuffites, aleurolites, sandstones; biotite–plagioclase and amphibole–biotite–plagioclase gneisses and migmatites; biotite–plagioclase gneisses with aluminiferous minerals; amphibole–biotite–plagioclase gneisses with pyroxene and pyroxene-amphibole–plagioclase crystalline schists; amphibolites and amphibole crystalline schists; differentiated basite–ultrabasites; microcline granites; amphibolites, pyroxene–amphibole–plagioclase schists, gneisses, granite–gneisses; main faults; geological boundaries; seismic boundaries.

of the deep parts of the Kola and KTB sections and to the thermodynamical conditions during progressive and regressive metamorphic transformations of the Kola series rocks.

Seismic methods are the primary source of information for the deep structure of the continental crust, and thus it is very important to learn to use seismic data for determination of deep seat rock permeability. For this purpose, we have to consider the parameters, depending on rock matrix, as well as on pore space properties. Anisotropy of elastic wave velocities correlated with rock permeability and its anisotropy may be used in this case. Preliminary results of the investigations carried out on the core samples from the Kola SG-3 and KTB superdeep boreholes (Kern et al., 1991; Zharikov et al., 1990) show that such relationships can be established. This conclusion also agrees with the results presented in Nikitin et al. (2001). So, with this in mind, we studied permeability anisotropy with the same system of coordinates that had been

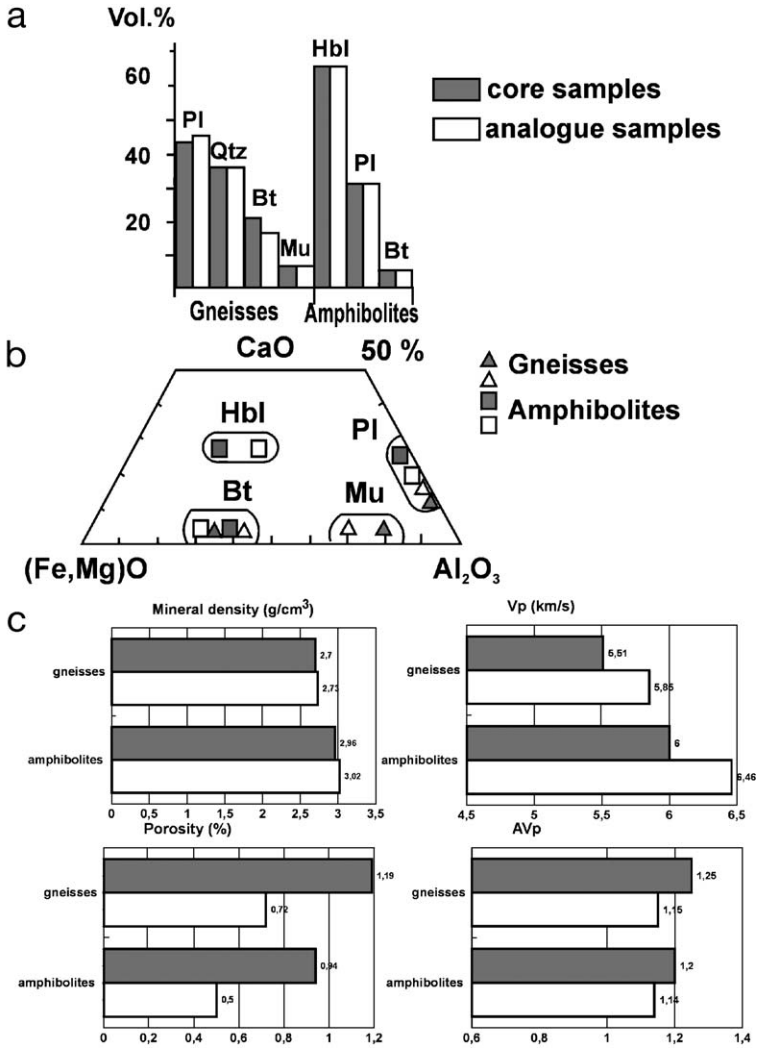

Fig. 2. Mean values of mineral composition (a); chemical composition of rock-forming minerals (b) and physical properties (c) of the studied Kola series core and surface analogue samples.

used by Kern et al. (2001) for seismic wave velocities: parallel and normal to foliation.

2. Geological setting and sample selection

The Kola superdeep borehole (SG-3) was drilled in a synformic structure located in the northeastern part of the Baltic Shield. It penetrates Proterozoic metavolcanic rocks lying on the Archean faulted basement—gneisses and amphibolites (Fig. 1). Both of these complexes are affected by regional progressive and regressive metamorphic transformations and transected by numerous faults. The details of geological settings of the SG-3 area are presented in Kozlovsky (1987). The KTB borehole penetrates the rocks of the Zone of Erbendorf-Vohenstrauss located in the western part of a Bohemian massif formed from a Late Proterozoic to Paleosoic sequence, transformed to amphibolites, metagabbros and associated metatuffites, and meta-ultra-mafics, as well as intercalated garnet-mica-gneisses of a turbid origin. Intrusion times and depositional ages are Early Ordovician, while poly-metamorphic overprints have been recorded between 500 and 320 Ma with the main amphibolite phase at about 400 Ma (Emmerman, 1990). Thus, comparing the geological data on SG-3 and KTB, one observes that the rocks with closely related composition, metamorphic grade and, probably, physical properties occur in both sections. However, samples of such rocks can be collected from the depth up to 8 km in the KTB section, from 7 to 12 km in SG-3 and due to the synformic structure of the SG-3 site from the Earth's surface, as well.

Eight samples of the typical rocks of the Kola series (amphibolites and gneisses) of the same amphibolite metamorphic facies with minimal regressive transformations were chosen for the experiments. The samples were collected from the depths of 8–11 km in intervals where the core underwent a minimal degree of disking. The surface samples–analogues were collected at the distance of 50 km to northeast of the borehole (Fig. 1). KTB was also presented by amphibolite. The sample was collected at the lower depth (3847 m).

The data obtained on core and surface Kola samples showed that their mineral assemblages are similar. However, the physical properties are different (Fig. 2). Thus, the mean values of rock mineral composition, the compositions of main rock-form-

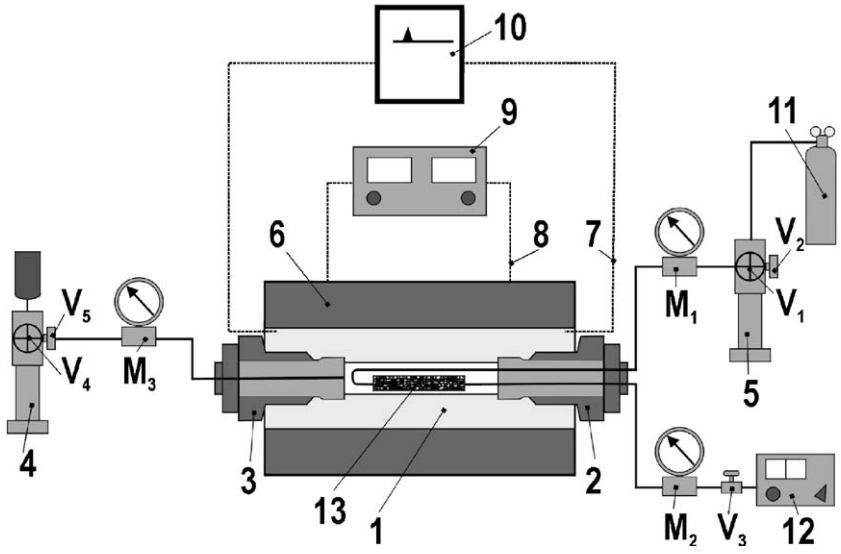

Fig. 3. Experimental setup for permeability measurements at high temperature and pressure. (1) High pressure vessel; (2, 3) obturators; (4, 5) screw presses; (6) furnace; (7, 8) thermocouples; (9) temperature controlling unit; (10) temperature recording unit; (11) gas reservoir; (12) flow volume measuring device; (13) sample jacketed by thin-wall tubes. M1–M3: gauges, V1–V5: valves.

ing minerals, the textures of rock forming minerals are similar and mineral density values are all similar. Porosity values of core samples are higher. Their V_p anisotropy values are also higher, but, in contrast, V_p values are lower. We attribute the differences to the effect of technogenic microcracks that appeared when core samples were drilled and lifted to the surface (Wolter and Berckhemer, 1989). The details on sample collection and the results of their geological, petrophysical and neutron diffraction studies performed are presented in Lobanov et al. (2002).

3. Experimental setups

The permeability measurements were carried out under pressure up to 150 MPa and temperature up to 600 °C using a hydrostatic setup (Fig. 3). A cylindrical sample of 9.6 mm in diameter and 15–20 mm in length jacketed by gold thin-wall tubes (13) is placed in high pressure vessel (1) and sealed by the obturators (2, 3). Confining pressure is produced by the screw press (4). Water is a pressure-transferring medium. Gas or water can be used as flowing fluid. When water is used; pore pressure is produced by the screw press (5); with gas flowing, it is shut off. In this case, argon under constant pressure within the range from 1 to 12 MPa controlled by the valve (V_2) flows from the reservoir (11) through the sample to the device measuring flow volume (12). Confining and pore pressures are measured by gauges M1–M3. Temperature is produced by the furnace (6), measured by thermocouples (7, 8), controlled by the unit (9) and recorded by the unit (10).

For observation of microcracking on the sample surface, a cell producing temperature up to 600 °C and pressure up to 100 MPa was used (Fig. 4). The cell materials were all non-magnetic. To insert wires and apply pressure, a special lock was constructed, with six electric vacuum entries and a through-going high-pressure capillary. The cell was attached to the lock by a thin capillary (1 and 0.2 mm in outside and inside diameter, respectively) twisted as a loop. A sample (4) in gold lining (5) is placed in the nut (2) of the screw chamber (1) and sealed by the lens-like ring (3). Pressure in the cell is produced and controlled by a micropress placed outside SEM and transferred by the capillary (7). Temperature is produced by furnace (8) and measured by the thermocouple (6).

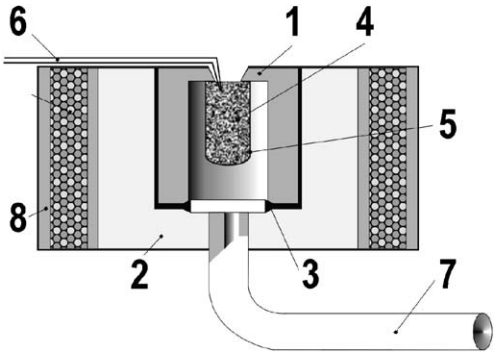

Fig. 4. Experimental cell for microstructure investigations under SEM at high temperature and pressure. (1) Screw chamber; (2) nut; (3) lens-like ring; (4) sample; (5) gold lining; (6) thermocouple; (7) capillary; (8) furnace.

4. Experimental procedure

In order to avoid any interaction between rock and pore fluid argon was chosen as flowing media. We applied the steady-state method with the Klinkenberg correction (Klinkenberg, 1941). Before using the technique, we conducted tests to be certain that it would remain valid at high temperatures. Klinkenberg proposed the dependence of the gas permeability (k_g) on gas pressure (p), permeability to water (k_w) and the constant characterizing pore size (b):

$$k_g = k_w\left(1+\frac{b}{p}\right), \quad (1)$$

Following this technique, a series of gas permeability determinations at different pore pressures was made in order to obtain the dependence $k_g = f(1/\bar{p})$. Then, it was extrapolated to $f(1/\bar{p}) = 0$ and desired k_w value was obtained.

We tried to find a way of running through the entire ranges of temperature and pressure during the experiment using a single sample with minimal damages in its structure. The following outline of PT changes was adopted: the given temperatures up to 600 °C had been reached on simultaneous heating and pressure increase, and permeability measurements during pres-

Table 1
Rock sample permeability (m^2)

	Sample	Rock	Temperature (°C)	Effective pressure (MPa)					
				30	50	80	100	120	150
1	31421	Gneiss	20	$5.80\cdot10^{-18}$	$3.70\cdot10^{-18}$	$9.80\cdot10^{-19}$	$9.20\cdot10^{-19}$	$9.00\cdot10^{-19}$	$7.70\cdot10^{-19}$
	Kola superdeep borehole	Mineral composition (vol.%)	100	$7.10\cdot10^{-18}$	$4.60\cdot10^{-18}$	$4.30\cdot10^{-18}$	$3.60\cdot10^{-18}$	$3.50\cdot10^{-18}$	$2.60\cdot10^{-18}$
	Collection	Pl = 40, Qtz = 35,	200	$6.50\cdot10^{-19}$	$4.20\cdot10^{-19}$	$4.00\cdot10^{-19}$	$3.50\cdot10^{-19}$	$3.30\cdot10^{-19}$	$3.20\cdot10^{-19}$
	depth 8812 m	Mc = 5, Ms = 7,	300	$4.80\cdot10^{-19}$	$1.80\cdot10^{-19}$	$1.60\cdot10^{-19}$	$1.40\cdot10^{-19}$	$1.10\cdot10^{-19}$	$8.80\cdot10^{-20}$
		Ep = 7, Bt = 5,	400	$5.80\cdot10^{-19}$	$1.60\cdot10^{-19}$	$2.40\cdot10^{-20}$	$6.80\cdot10^{-21}$	$5.00\cdot10^{-21}$	$4.00\cdot10^{-21}$
		Spn, Carb = 1	500	$1.60\cdot10^{-18}$	$1.60\cdot10^{-19}$	$5.60\cdot10^{-19}$	$2.00\cdot10^{-21}$	$1.00\cdot10^{-23}$	$1.00\cdot10^{-23}$
	Flow II to foliation	Initial porosity = 2.01%	600	$1.50\cdot10^{-17}$	$4.10\cdot10^{-18}$	$1.20\cdot10^{-18}$	$5.80\cdot10^{-19}$	$2.80\cdot10^{-19}$	$1.50\cdot10^{-19}$
2	31421	Gneiss	20	$1.10\cdot10^{-17}$	$7.30\cdot10^{-18}$	$4.20\cdot10^{-18}$	$3.00\cdot10^{-18}$	$2.40\cdot10^{-18}$	$1.00\cdot10^{-18}$
	Kola superdeep borehole	Mineral composition (vol.%)	100	$1.80\cdot10^{-18}$	$1.40\cdot10^{-18}$	$1.10\cdot10^{-18}$	$7.90\cdot10^{-19}$	$6.20\cdot10^{-19}$	$3.50\cdot10^{-19}$
	Collection	Pl = 40, Qtz = 35,	200	$1.30\cdot10^{-19}$	$1.30\cdot10^{-19}$	$<10^{-23}$	$<10^{-23}$	$<10^{-23}$	$<10^{-23}$
	depth 8812 m	Mc = 5, Ms = 7,	300	$2.30\cdot10^{-19}$	$7.70\cdot10^{-20}$	$3.50\cdot10^{-20}$	$2.30\cdot10^{-20}$	$1.00\cdot10^{-20}$	$8.00\cdot10^{-21}$
		Ep = 7, Bt = 5, Spn,	400	$9.90\cdot10^{-20}$	$2.00\cdot10^{-20}$	$1.10\cdot10^{-20}$	$5.20\cdot10^{-21}$	$5.00\cdot10^{-21}$	$<10^{-23}$
		Carb = 1	500	$2.80\cdot10^{-19}$	$1.20\cdot10^{-19}$	$1.90\cdot10^{-20}$	$1.20\cdot10^{-20}$	$3.50\cdot10^{-21}$	$2.50\cdot10^{-21}$
	Flow II to foliation	Initial porosity = 2.01%	600	$5.20\cdot10^{-19}$	$1.80\cdot10^{-19}$	$4.40\cdot10^{-20}$	$3.00\cdot10^{-20}$	–	$2.2\cdot10^{-20}$
3	P-19	Gneiss	20	$8.00\cdot10^{-18}$	$7.40\cdot10^{-18}$	$6.90\cdot10^{-18}$	$4.40\cdot10^{-18}$	$4.00\cdot10^{-18}$	$4.10\cdot10^{-18}$
	Kola, surface	Mineral composition (vol.%)	100	$2.40\cdot10^{-18}$	$2.10\cdot10^{-18}$	$1.80\cdot10^{-18}$	$1.70\cdot10^{-18}$	$1.50\cdot10^{-18}$	$1.50\cdot10^{-18}$
		Pl = 50, Qtz = 35,	200	$2.10\cdot10^{-18}$	$2.10\cdot10^{-18}$	$2.80\cdot10^{-18}$	$2.70\cdot10^{-18}$	–	$2.40\cdot10^{-18}$
		Bt = 10 Ms = 4, Spn, Carb = 1	300	$2.70\cdot10^{-18}$	–	$2.70\cdot10^{-18}$	–	$2.50\cdot10^{-18}$	$2.20\cdot10^{-18}$
	Flow II to foliation	Initial porosity = 1.16%	400	$3.70\cdot10^{-18}$	–	$3.20\cdot10^{-18}$	–	$2.70\cdot10^{-18}$	$2.50\cdot10^{-18}$
4	31571	Amphibolite	20	–	$9.00\cdot10^{-18}$	$2.20\cdot10^{-18}$	$1.50\cdot10^{-18}$	$5.00\cdot10^{-19}$	$2.00\cdot10^{-19}$
	Kola superdeep borehole	Mineral composition (vol.%)	100	$5.50\cdot10^{-17}$	$4.20\cdot10^{-17}$	$1.80\cdot10^{-17}$	$1.70\cdot10^{-17}$	$2.60\cdot10^{-17}$	$5.50\cdot10^{-18}$
	Collection	Hbl = 60, Pl = 35,	200	$4.80\cdot10^{-18}$	$5.70\cdot10^{-18}$	$7.10\cdot10^{-18}$	$6.60\cdot10^{-18}$	$5.80\cdot10^{-18}$	$7.20\cdot10^{-18}$
	depth 8863 m	Spn = 5, Carb = 1	300	$8.90\cdot10^{-20}$	$5.60\cdot10^{-20}$	$2.90\cdot10^{-20}$	$1.90\cdot10^{-20}$	$1.80\cdot10^{-20}$	$1.80\cdot10^{-20}$
			400	$4.90\cdot10^{-20}$	–	$6.10\cdot10^{-21}$	$4.90\cdot10^{-21}$	$3.50\cdot10^{-21}$	$1.60\cdot10^{-21}$
			500	$4.80\cdot10^{-20}$	$2.50\cdot10^{-20}$	$1.30\cdot10^{-20}$	$3.50\cdot10^{-20}$	$1.60\cdot10^{-20}$	$1.00\cdot10^{-22}$
	Flow II to core axis	Initial porosity = 1.46%	600	$5.30\cdot10^{-19}$	$1.50\cdot10^{-19}$	$4.20\cdot10^{-20}$	$5.30\cdot10^{-20}$	$4.00\cdot10^{-20}$	$3.00\cdot10^{-20}$
5	31863	Amphibolite	20	–	$7.50\cdot10^{-18}$	$1.10\cdot10^{-17}$	$1.20\cdot10^{-17}$	–	$1.60\cdot10^{-17}$
	Kola superdeep borehole	Mineral composition (vol.%)	100	$7.80\cdot10^{-17}$	$5.80\cdot10^{-17}$	$3.00\cdot10^{-17}$	$3.00\cdot10^{-17}$	$1.40\cdot10^{-17}$	$8.70\cdot10^{-18}$
	Collection	Hbl = 65, Pl = 25,	200	–	$5.00\cdot10^{-21}$	$2.00\cdot10^{-22}$	$1.00\cdot10^{-22}$	$1.00\cdot10^{-22}$	$1.00\cdot10^{-22}$
	depth 8930 m	Spn = 5, Carb, Ep,	300	$1.50\cdot10^{-19}$	$3.70\cdot10^{-20}$	$1.40\cdot10^{-20}$	$6.00\cdot10^{-21}$	$1.00\cdot10^{-22}$	$1.00\cdot10^{-22}$
		Ore = 5	400	$2.60\cdot10^{-19}$	$5.90\cdot10^{-19}$	$3.40\cdot10^{-20}$	–	$8.00\cdot10^{-21}$	$1.00\cdot10^{-22}$
			500	$2.80\cdot10^{-20}$	–	$9.20\cdot10^{-21}$	$1.00\cdot10^{-22}$	$1.00\cdot10^{-22}$	$1.00\cdot10^{-22}$
	Flow II to foliation	Initial porosity = 1.56%	600	$7.60\cdot10^{-19}$	$2.30\cdot10^{-19}$	$9.20\cdot10^{-20}$	$2.00\cdot10^{-20}$	$2.30\cdot10^{-20}$	$9.30\cdot10^{-21}$
6	31863	Amphibolite	20	$1.60\cdot10^{-17}$	$1.10\cdot10^{-17}$	$1.00\cdot10^{-17}$	$1.10\cdot10^{-17}$	$1.80\cdot10^{-17}$	$1.70\cdot10^{-18}$
	Kola superdeep borehole	Mineral composition (vol.%)	100	$1.60\cdot10^{-17}$	$8.10\cdot10^{-17}$	$4.40\cdot10^{-18}$	$2.40\cdot10^{-18}$	$3.50\cdot10^{-18}$	$1.90\cdot10^{-18}$
	Collection	Hbl = 65, Pl = 25,	200	$5.40\cdot10^{-18}$	$3.90\cdot10^{-18}$	$3.40\cdot10^{-18}$	$2.00\cdot10^{-18}$	$1.90\cdot10^{-18}$	$9.20\cdot10^{-18}$
	depth 8940 m	Spn = 5, Carb, Ep,	300	$1.40\cdot10^{-18}$	$4.80\cdot10^{-20}$	$2.30\cdot10^{-20}$	$1.50\cdot10^{-20}$	$4.80\cdot10^{-21}$	$6.30\cdot10^{-22}$
		Ore = 5	400	$9.90\cdot10^{-20}$	$2.00\cdot10^{-20}$	$1.10\cdot10^{-20}$	$5.20\cdot10^{-21}$	$5.00\cdot10^{-21}$	$1.00\cdot10^{-21}$
			500	$2.80\cdot10^{-19}$	$6.00\cdot10^{-20}$	$2.10\cdot10^{-20}$	$1.20\cdot10^{-20}$	$1.10\cdot10^{-20}$	$1.00\cdot10^{-22}$

Table 1 (*continued*)

	Sample	Rock	Temperature (°C)	Effective pressure (MPa)					
				30	50	80	100	120	150
6	Flow + to foliation	Initial porosity = 1.56%	600	$5.20\cdot10^{-19}$	$1.80\cdot10^{-19}$	$4.40\cdot10^{-20}$	$3.00\cdot10^{-20}$	–	$2.20\cdot10^{-20}$
7	43639	Amphibolite	20	$3.00\cdot10^{-17}$	$1.80\cdot10^{-17}$	$1.10\cdot10^{-17}$	$8.50\cdot10^{-18}$	$6.00\cdot10^{-18}$	$2.10\cdot10^{-18}$
	Kola superdeep borehole	Mineral composition (vol.%)	100	$1.80\cdot10^{-17}$	$1.10\cdot10^{-17}$	$7.50\cdot10^{-18}$	$6.60\cdot10^{-18}$	$4.90\cdot10^{-18}$	$5.50\cdot10^{-18}$
	Collection depth 11 400 m	Hbl = 55, Pl = 40,	200	$4.10\cdot10^{-19}$	$1.80\cdot10^{-19}$	$4.90\cdot10^{-20}$	$6.20\cdot10^{-20}$	$5.60\cdot10^{-20}$	$4.90\cdot10^{-20}$
		Bt = 2, Qtz = 2, Ep,	300	$6.10\cdot10^{-20}$	$4.90\cdot10^{-20}$	$1.60\cdot10^{-20}$	$1.50\cdot10^{-20}$	$2.00\cdot10^{-20}$	$2.50\cdot10^{-20}$
		Carb, Ore = 1	400	$1.20\cdot10^{-19}$	$9.40\cdot10^{-20}$	$1.00\cdot10^{-20}$	$1.40\cdot10^{-20}$	$6.90\cdot10^{-20}$	$1.50\cdot10^{-21}$
			500	$4.60\cdot10^{-19}$	$1.20\cdot10^{-19}$	$1.90\cdot10^{-20}$	$1.20\cdot10^{-20}$	$3.50\cdot10^{-21}$	$2.50\cdot10^{-21}$
	Flow II to core axis	Initial porosity = 1.80%	600	$4.20\cdot10^{-18}$	$1.00\cdot10^{-18}$	$3.80\cdot10^{-19}$	$1.80\cdot10^{-19}$	$1.00\cdot10^{-19}$	$9.10\cdot10^{-20}$
8	P-61	Amphibolite	20	$1.40\cdot10^{-18}$	$1.10\cdot10^{-18}$	$8.80\cdot10^{-19}$	$9.20\cdot10^{-19}$	–	$2.70\cdot10^{-19}$
	Kola, surface	Mineral composition (vol.%)	100	$1.40\cdot10^{-18}$	$9.40\cdot10^{-19}$	$8.40\cdot10^{-19}$	$8.00\cdot10^{-19}$	$7.60\cdot10^{-19}$	$5.30\cdot10^{-19}$
		Hbl = 70, Pl = 25,	200	$8.00\cdot10^{-20}$	$8.00\cdot10^{-20}$	$7.00\cdot10^{-20}$	$7.00\cdot10^{-20}$	–	$5.00\cdot10^{-20}$
		Qtz = 2, Bt = 2, Cl,	300	$7.00\cdot10^{-19}$	$6.80\cdot10^{-20}$	$4.10\cdot10^{-20}$	$1.80\cdot10^{-20}$	–	$4.10\cdot10^{-22}$
		Ep, Sph = 1	400	$9.00\cdot10^{-20}$	$9.10\cdot10^{-20}$	$2.40\cdot10^{-20}$	$1.20\cdot10^{-20}$	$<10^{-23}$	$<10^{-23}$
			500	$4.00\cdot10^{-21}$	$4.00\cdot10^{-21}$	$1.00\cdot10^{-21}$	$<10^{-23}$	$<10^{-23}$	$<10^{-23}$
	Flow II to foliation	Initial porosity = 0.96%	600	$2.70\cdot10^{-20}$	$2.70\cdot10^{-20}$	$3.00\cdot10^{-21}$	$8.00\cdot10^{-23}$	$<10^{-23}$	$<10^{-23}$
9	941 Glp	Amphibolite	20	$1.01\cdot10^{-17}$	$9.94\cdot10^{-18}$	$8.78\cdot10^{-18}$	$7.65\cdot10^{-18}$	$4.45\cdot10^{-18}$	$1.10\cdot10^{-18}$
	KTB, Pilot borehole	Mineral composition (vol.%)	100	$2.07\cdot10^{-18}$	$1.50\cdot10^{-18}$	$9.92\cdot10^{-19}$	$8.61\cdot10^{-19}$	$6.50\cdot10^{-19}$	$2.90\cdot10^{-19}$
	Collection depth 3847 m	Pl = 44, Hbl = 39,	200	$5.14\cdot10^{-19}$	$4.70\cdot10^{-19}$	$4.02\cdot10^{-19}$	$3.00\cdot10^{-19}$	$2.30\cdot10^{-19}$	$1.33\cdot10^{-19}$
		Sc = 7, Bt = 4,	300	$<10^{-23}$	$<10^{-23}$	$<10^{-23}$	$<10^{-23}$	$<10^{-23}$	$<10^{-23}$
		Mag = 3, Qtz = 1	400	$4.50\cdot10^{-20}$	$1.60\cdot10^{-20}$	$1.00\cdot10^{-20}$	$1.00\cdot10^{-21}$	$<10^{-23}$	$<10^{-23}$
			500	$4.00\cdot10^{-21}$	$1.00\cdot10^{-21}$	$<10^{-23}$	$<10^{-23}$	$<10^{-23}$	$<10^{-23}$
	Flow II to core axis	Initial porosity = 0.99%	600	$1.00\cdot10^{-20}$	$5.86\cdot10^{-21}$	$9.18\cdot10^{-21}$	$<10^{-23}$	$<10^{-23}$	$<10^{-23}$

$<10^{-23}$ means that gas discharge measured during 1 day did not reach sensitivity of the volumeter = 0.02 cm^3 (about 7 cm^3/year), that corresponds to the permeability value of 10^{-23} m^2.

sure cycles at constant temperature were then performed. This method allowed us to obtain up to 42 permeability values at various PT during the tests on each sample.

5. Experimental results

5.1. Temperature and pressure dependencies of permeability

The experimental results obtained with flow parallel, normal to foliation or normal to core axis are presented in Table 1. It can be seen that within the entire pressure and temperature ranges permeability varies up to many decimal orders. We have not found any correlation between permeability and rock type, but we found a few common tendencies of permeability behavior related to depth of sampling and flow direction. Same typical trends obtained are presented in Figs. 5 and 6.

Rock sample permeability decreases with a confining pressure increase (Fig. 5). The results agree with the data presented in Morrow et al. (1994). The trend gradient rises with increasing temperature and pressure. Generally, behavior of permeability trends obtained does not depend on flow direction.

The temperature–permeability trends obtained with flow parallel and normal to foliation are slightly different (Fig. 6d). As a rule, with flow parallel to foliation, the values of permeability are higher than with flow normal to foliation.

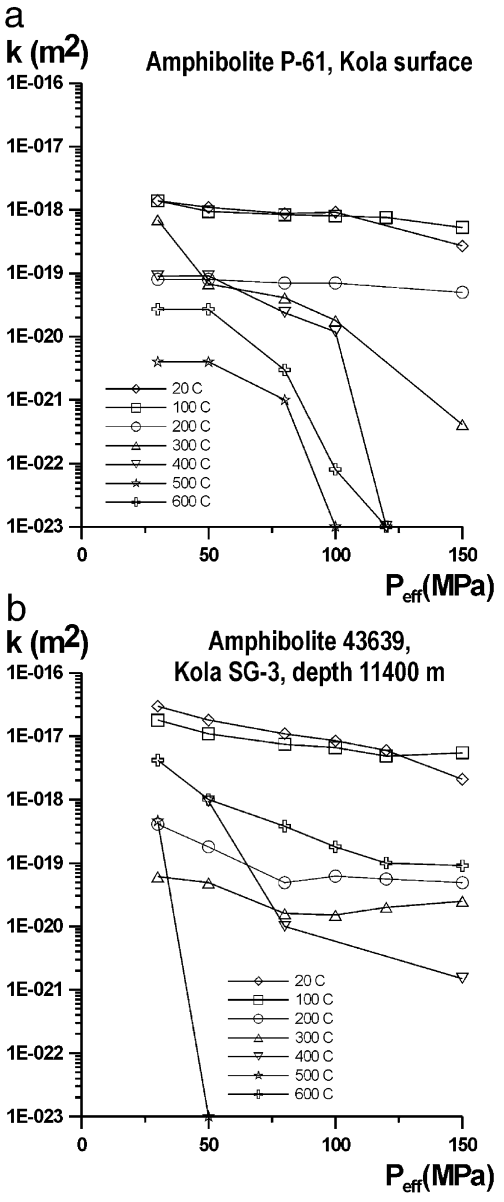

Fig. 5. Effective pressure dependencies of permeability.

However, what is more essential, temperature–permeability trend behavior clearly depends on effective pressure and depth of sample selection.

- At low P_{eff} (30–80 MPa), a temperature increase leads first to permeability decrease and then to its increase. These temperature trends inversions occur at temperatures of 200–500 °C (Fig. 6a–c).
- At higher P_{eff} (100–150 MPa), the temperature trends of the samples selected at great depths (8–11 km) also have inversions (Fig. 6c). In contrast, permeability of the samples selected at shallow depth (3.8 km) and on the surface decreases within the entire temperature range (Fig. 6a,b).

Permeability anisotropy (A_k), calculated analogously to V_p anisotropy (Birch, 1961):

$$A_k = \frac{|k_{\text{II}} - k_{+}|}{k_{\text{mean}}} \cdot 100(\%), \qquad (2)$$

(where k_{II} and k_{+} are permeability values with flow parallel and normal to foliation, respectively, and k_{mean} is its mean value) increases with temperature, reaches a maximum at 200 °C and then decreases (Fig. 7).

5.2. Microstructure study results and the origin of permeability behavior at high PT

In order to explain the data obtained, we carried out microstructure investigations using a specially designed cell described above. The cell is capable of producing temperature up to 600 °C and pressure up to 100 MPa. For direct observation of sample surface at high PT, this entire cell can be placed into a scanning electron microscope.

Our primary interest was understanding why the temperature trends change and why such unidirectional action as heating causes permeability decrease and then its increase even under constant pressure. The observations showed the intensive microcrack initiation and closure correlating with permeability changes. There are two families of microcracks in the samples: with low aspect ratio (0.002–0.007), crossing several mineral grains and with high aspect ratio (0.03–0.05) located at the mineral grain boundaries. Their effect on rock permeability varies with temperature.

As an example, a fragment of microcrack on the surface of amphibolite core sample 43639 is given in Fig. 8. Such long, low aspect ratio (0.005) microcracks are typical of core samples collected at great depths (Fig. 10a). It is quite possible that they are of a technogenic origin. With temperature elevation from 100 to 300 °C at constant pressure of 80 MPa, the

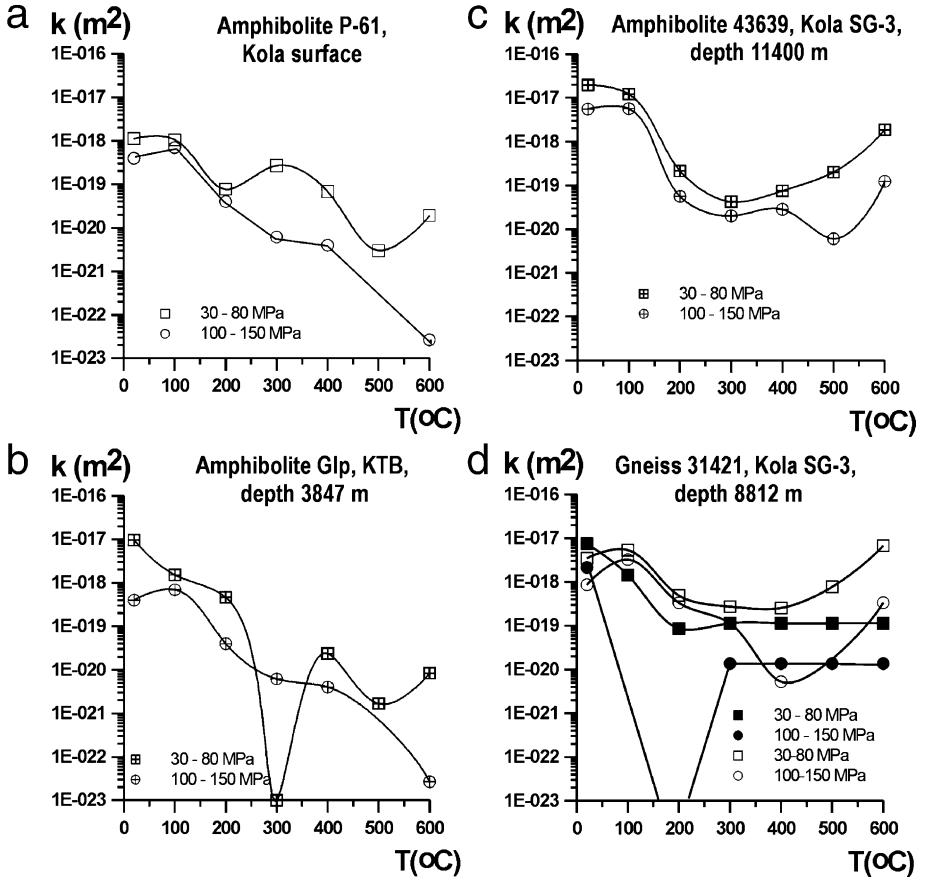

Fig. 6. Temperature dependencies of permeability (averaged by low and high P_{eff}).

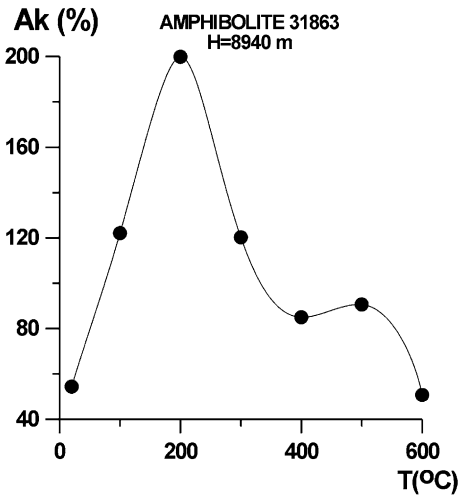

Fig. 7. Temperature dependence of permeability anisotropy.

mean aperture of the microcrack decreases from 2.5 to 1.3 μm. When heated up to 500 °C, the microcrack almost fully disappears: its aperture decreases up to 0.3 μm. The decrease of microcrack apertures correlates with sample permeability decrease from $7.5{\cdot}10^{-18}$ m^2 at 100 °C to $1.6{\cdot}10^{-20}$ m^2 at 300 °C (Table 1 and Fig. 6c).

In the paper (Dodrynin, 1970), a ratio permitting to estimate changes in microcrack aperture (δb) is presented as:

$$\delta b = \frac{2(1-\nu_m^2)(\sigma - p)}{3(1-2\nu_m)} l\beta_m, \quad (3)$$

where $(\sigma - p)$ = effective pressure, ν_m = rock matrix Poisson's ratio, β_m = rock matrix compressibility, l = microcrack length. In the course of the experiment, effective pressure has not been changing while heat-

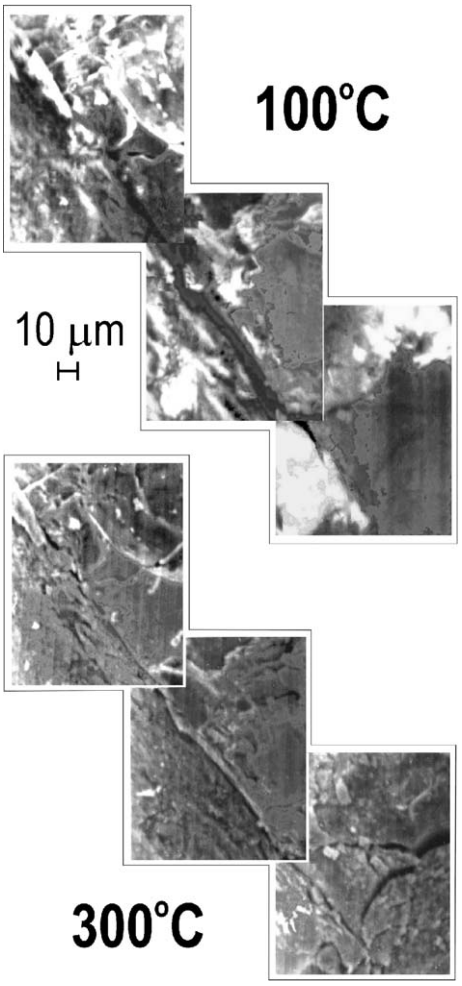

Fig. 8. Long microcrack closure in amphibolite core sample 43639 (depth: 11 400 m) on heating at $P = 80$ MPa.

ing. However, on being heated up to 300 °C, compressibility of rock matrix increases several times (Volarovich, 1988). For $l = 100$ μm, $\nu_m = 0.3$, $(\sigma - p) = 80$ MPa, $\beta_m = 2 \cdot 10^{-12}$ and $6 \cdot 10^{-12}$ Pa^{-1}, we obtain the aperture decrease of about 1.9 μm in good agreement with the data obtained under SEM. So, we can attribute the observed microcrack behavior to the dominating influence of effective pressure while rock matrix compressibility increases with heating. Looking at the whole surface of the sample, we can see that such long microckracks are relatively rare and randomly distributed. However, these microckracks, owing to their wide aperture (1–3 μm) make a considerable contribution to initial sample permeability, but because of high length (200–500 μm) they are unstable. As can be seen from Eq. (3), the change in aperture of microcrack is proportional to its length. Due to wall roughness they do not close completely under pressure: they divide into many small fragments. Nevertheless, a pore network misses its interconnectivity. Hence, permeability sharply decreases, as it was shown in Fig. 6.

Under such conditions, flow can channel through the high aspect ratio microcracks located at the grain boundaries, which are shorter and more stable (Fig. 10b). With increasing temperature, the values of thermal stress also increase and can overcome confining pressure effect. As a result, permeability also increases due to microcrack generation. There are two main backgrounds for crack generation: the first one—thermal stress concentration near the pre-existing microckracks, which are not completely closed; the second and principal one—microcrack generation at mineral grain boundaries (Figs. 9 and 10c).

Fig. 11 presents the results of permeability calculations for the high and low aspect ratio microcracks on heating (Shmonov et al., 1995). A simple model was based on mathematical analogies of Ohm and Darcy laws similar to those described in (Chida and Tanaka, 1983). Low aspect ratio microcracks close, whereas high aspect ratio ones open. Total effect of the superposition of these simultaneously running processes is expressed by the appearance of minima in the permeability–temperature trends.

From these observations and calculations, we can conclude that competitive effects of confining pressure and temperature, leading to microcrack opening and closure, cause the appearance of inversions in the permeability–temperature trends.

Using the results of the microstructure study, we also can propose an explanation of the observed changes in anisotropy (Fig. 7). We have studied core samples lifted from great depth in which an abundance of low aspect ratio microcracks, probably of a technogenic origin, were observed. They are randomly distributed and, as a result, anisotropy values of initial samples are low (Fig. 10a). At temperature of 200–300 °C they close. Only microcracks on the grain boundaries stay open and could serve as fluid channels. At the same time, anisotropy value increases. This probably reflects an effect of

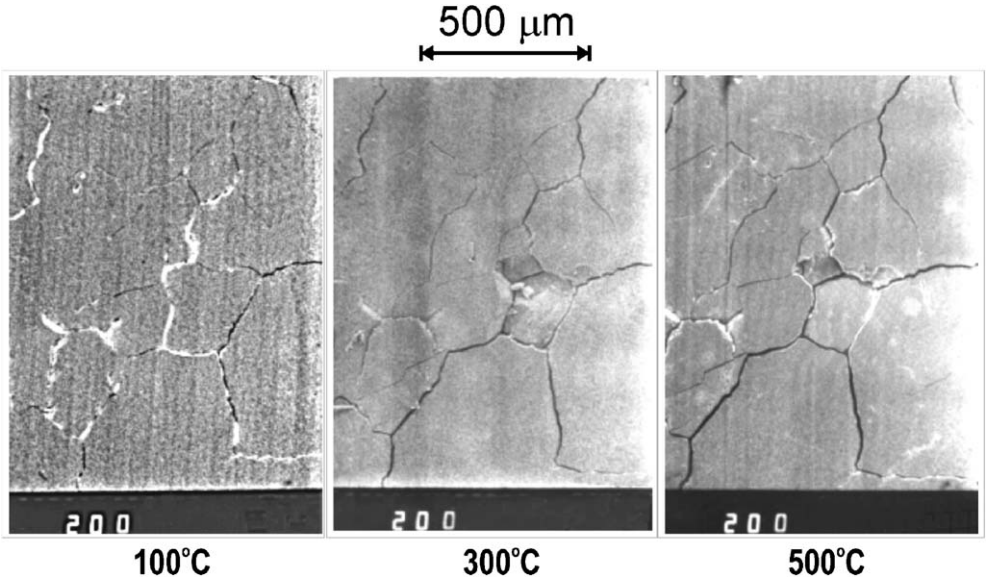

Fig. 9. Microcrack opening at the mineral grain boundaries on heating (P = 100 MPa).

microcracks oriented parallel to foliation along the grain boundaries of rock-forming minerals (Fig. 10b). Hence, at such PT, corresponding to the deep part of the Kola superdeep borehole section, the origins of the permeability anisotropy and anisotropy of elastic wave velocities also controlled by preferred orientation of rock-forming minerals (Kern et al., 2001), are similar. On heating to the higher temperatures (500–600 °C) microcracks at the mineral grain boundaries make rock structure so unsteady that minerals preferred orientations cease to be effective and permeability anisotropy decreases (Fig. 10c).

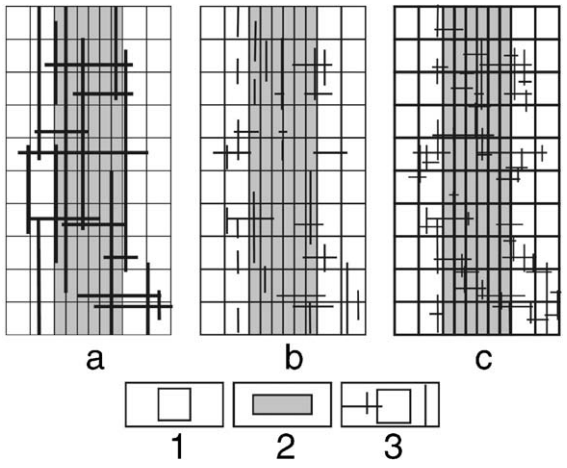

Fig. 10. Schematic sketch of microcrack closure and opening on heating. (1) Randomly oriented mineral grains, (2) mineral grains with preferred orientation, (3) microcracks.

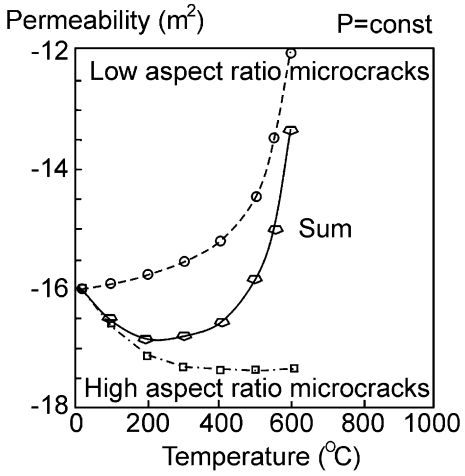

Fig. 11. Microcrack permeability on heating at P = constant; the results of numerical simulation.

6. Implication of the experimental results to the continental crust

The main goal of the study was to estimate in situ permeability of the Kola SG-3 rocks and their paleo-permeability during progressive and regressive metamorphism. Fig. 12a presents the permeability dependencies obtained with simultaneous increase of temperature and pressure simulating in situ conditions. PT of the experiments are listed in the right axis of the figure. The following assumptions were used when this PT-outline of experiments was chosen. If confining pressure is equal to lithostatic (P_{lit}) and fluid pressure is equal to hydrostatic (P_f), changes of effective pressure (P_{eff}) with depth can be derived as:

$$P_{eff} = (\rho_m - \rho_f)gh, \quad (4)$$

where ρ_m and ρ_f are the densities of mineral matrix and fluid, respectively, g = acceleration of gravity and h = depth. We assumed ρ_m equal to 2.84 g/cm^3 as the mean density of the SG-3 rocks (Kozlovsky, 1987). Unfortunately, the information on fluid salinity in the bottom part of the SG-3 section (>8 km) is minor. However, the available data evidence the low salinity (as a rule, its values are lower than 0.5 g/l; only in a few depth intervals they increase up to 2–3 g/l) (Kozlovsky, 1987). So, we assumed that ρ_f = 1.0 g/cm^3. Then, Eq. (4) was modified as:

$$P_{eff} = 1.84gh. \quad (5)$$

Temperature was changed in accordance with the mean value of geothermal gradient in the SG-3 borehole = 18 °C/km (Kozlovsky, 1987).

At the initial PT, permeability of core samples is 1–2 decimal orders higher than of the surface one. We attribute it to the effect of technogenic microcracks. With temperature and pressure increase permeability decreases. The gradients of the trends are different. So, it is possible to sort them into two families. The first one—with low values (10^{-21}–10^{-20} m^2)—gneiss 31421, core sample, flow normal to foliation and surface sample P-61. The second one—with higher values (10^{-19}–10^{-18} m^2) under conditions of great depths—the same gneiss sample, but with flow parallel to foliation and core sample 43639 with flow parallel to core axis. In samples of the first group, the minimal values of permeability are probably close to intrinsic rock properties due to minimal conservation of microcracks. In samples of the second group, at the same PT, microcracks stay open and, as a result, permeability values are higher. In this case, these could be cracks at grain boundaries and parallel to foliation and the remains of technogenic microcracks. As can be seen from the figure, with flow parallel to foliation, the permeability of gneiss sample 31421 decreases intensively than with flow normal to foliation. So, anisotropy increases with depth (Fig. 12b).

Certainly, the quantity of the studied samples is not enough to propose a detailed permeability profile of

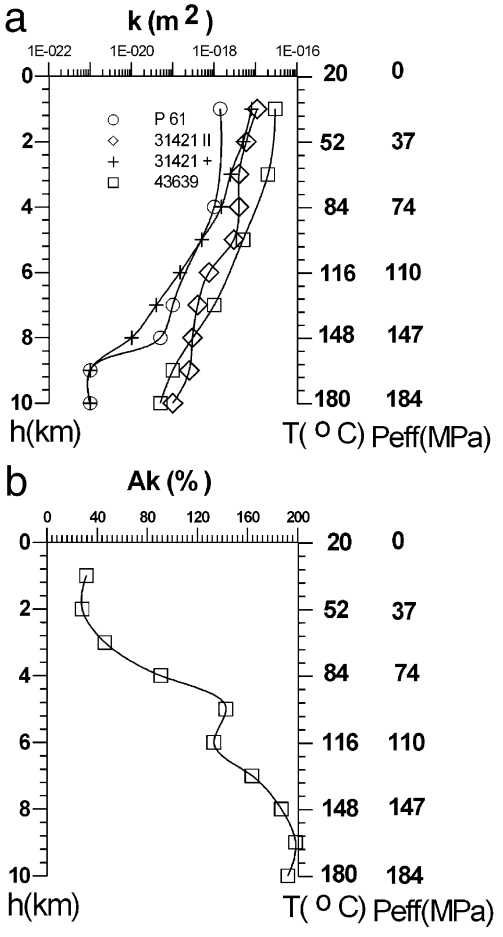

Fig. 12. Depth dependencies of permeability (a) and permeability anisotropy (b).

the SG-3 section. However, a few common tendencies could be marked. Permeability decreases with depth. Nevertheless, at PT, corresponding to great depths, its values can differ strongly (10^{-21}–10^{-19} m^2). Hence, we believe that at such depths a presence of local aquifer caused by rock matrix permeability difference is quite possible. To specify the data obtained and to evaluate a probable flow rate, it is necessary to know the pore pressure and fluid head values. Unfortunately, there are no such data on SG-3 currently available. We hope that the investigations being carried out there will be successful and such information will be forthcoming. So, using the data of the KTB investigations (Huenges, 1993; Huenges et al., 1997) for the first iteration, we chose the most realistic variant of pore pressure profile: hydrostatic one.

Another important issue is how to account a scale effect. Considering the laboratory data and the data of the tests in the shallow boreholes Brace found that permeability of rock massif could be three decimal orders higher than that as measured on the samples due to fracture occurrence (Brace, 1980). However, it is not clear is this trend true under conditions of great depths. Therefore, the convincing data on fracture occurrence at great depth are not still available. According to the results of the tests carried out in SG-3 at the depth of 6170–6470 m (Kozlovsky, 1987), permeability value is very low: of about $2{\cdot}10^{-19}$ m^2 and from our experimental data at PT conditions of such depths permeability ranges from 10^{-19} to 10^{-17} m^2 (Fig. 12a). In the depth interval of 9031–9131 m in KTB, permeability ranges from 5 to $13{\cdot}10^{-18}$ m^2 (Huenges et al., 1997). According to our experimental data obtained at temperature of about 250 °C and effective pressure of about 150 MPa, corresponding to PT conditions of 9 km depth in KTB, permeability ranges from $4.5{\cdot}10^{-21}$ to $2.3{\cdot}10^{-18}$ m^2. In Huenges et al. (1997), it was shown that, in the case of superdeep borehole studies, the scale problem is not restricted by transfer from sample dimensions to larger dimensions of rock massif. The detailed knowledge of hydrogeological situation in the borehole area is of critical importance. We mean fluid origin and composition, temperature and pressure profiles; first of all, a formation pressure profile. Correlating data on SG-3 and KTB, one can see that they have something in common. A presence of fluids was revealed in the both boreholes at the depth previously considerable as unreachable for them (up to 9 km in KTB and up to 11 km in SG-3). At the same time in KTB, it was found a hydraulic communication between the deep fracture zone at the depth of about 9.1 km with shallow fracture zones (Huenges et al., 1997). But in the SG-3 section, the aquifers connected with near-surface ones were found only at the depth up to 4.5 km. The deeper aquifers are confined and their origin is unclear. It can be fracture zones. However, the experimental data we obtained evidence that occurrence of such deep aquifer can be caused also by rock matrix permeability variations.

Thus, the origin of subhorizontal seismic boundaries at the depths of 10–15 km in the SG-3 site is still under discussion. They are considered to be associated with fracture zones, but there is an opposite opinion that unbroken rocks occur at such depths and the seismic reflections are related to rock fabric anisotropy. In this case, it is unclear why they are discordant with Kola series rocks dipping in the range from 28° to 45°, sometimes up to 70° to SSW (Kozlovsky, 1987, Kazansky et al., 1985). It seems reasonable that appearance of such reflections can be caused by recent stress conditions in the eastern part of the Baltic Shield. These zones may be associated with fluids, but they can differ strongly in fluid regime: filtration runs alternately through large fracture zones or through microcracks.

The rocks of the Kola series underwent progressive and regressive metamorphic transformations. Those were sequential processes of the geological time scale and so it is impossible to render them in laboratory conditions. Also, we admit that the water–rock interaction was not simulated. However, it is well known that the type of water–rock interaction on micro scale: in pores and microcracks, and on macro scale: in fractures, strongly differs. In the first case, it leads to geochemical transformations of the whole volume of rock and, in the second case, it is limited by crack sealing and vein development. The experimental results obtained allow to divide the pathways of fluids at PT of progressive and regressive metamorphism.

Progressive metamorphic transformations of the Kola series took place at temperature of about 500–600 °C and fluid pressure close to the lithostatic (Kazansky, 1988, 1992; Kazansky et al., 1985). Hence, effective pressure was low. At temperature of 500–600 °C and low effective pressure sample

permeability is from 10^{-19} to 10^{-18} m^2 (Table 1). Under such conditions, fluid flow could penetrate through the whole volume of rock.

In the rocks of the SG-3 section, the regressive metamorphiñ transformations at temperatures of about 180–320 °C were found (Kazansky, 1988; Kazansky et al., 1985; Kozlovsky, 1987). At these temperatures, the obtained permeability values (Table 1) are a few decimal orders lower ($<10^{-21}$ m^2), so fluid flow could be concentrated in the large fracture zones only. It is indicative that hydrothermal sulfide mineralization is related to the zones of dislocations and cataclase.

7. Conclusions

Permeability of the samples collected from the surface and from the depths of 8–11 km in the Kola SG-3 and from the depth of 3.8 in the KTB boreholes was studied at temperatures up to 600 °C and pressures up to 150 MPa. These PT correspond to in situ conditions of the deep parts of the superdeep boreholes and to the conditions of progressive and regressive metamorphism of the Kola series rocks. The experiments were carried out with fluid filtration parallel and normal to rock foliation and parallel to core axis. The following conclusions have been reached from the study:

1. Increase of confining pressure leads to a decrease of rock permeability.

2. Temperature–permeability trend behavior depends on effective pressure and depth of sample selection:

- At low P_{eff} (30–80 MPa), a temperature increase leads first to permeability decrease and then to its increase. The temperature trends inversions occur at temperatures of 200–500 °C.
- At higher P_{eff} (100–150 MPa), the temperature trends of the samples selected at great depths (8–11 km) also have inversions. In contrast, permeability of the samples selected at shallow depth (3.8 km) and on the surface decreases within the entire temperature range.

As a rule, with flow parallel to foliation the values of permeability are higher than with flow normal to foliation.

3. The results of microstructure studies allow to conclude that microcrack initiation and closure, due to a competitive influence of temperature and pressure cause such permeability behavior. In the samples there are two families of microcracks: those with low aspect ratio ones, crossing several mineral grains and with high aspect ratio ones, localized at the boundaries of mineral grains. The effect of these microcracks on rock permeability changes with temperature. On sample heating the microcracks with low aspect ratio close and microcracks with high aspect ratio open. As a result, total effect is expressed in appearance of inversions on the permeability–temperature trends.

4. Permeability anisotropy increases with temperature, reaches a maximum at 200 °C and then decreases. Under in situ PT of deep parts of the Kola SG-3 section, the permeability anisotropy is controlled by preferred orientation of main rock-forming minerals. Hence, at such conditions, the origins of elastic wave velocities and permeability anisotropies are similar.

5. With depth, sample permeability decreases with different gradients. As a result, at PT of great depth two families of trends could be distinguished by values. Very low permeability values (close to intrinsic rock properties) are due to minimal microcracks conservation. Higher permeability values are due to microcracks systems holding out at the same PT. Thus, it could be assumed that deep seat rocks can vary greatly in permeability and against the common background of permeability decrease with depth local deep aquifers may occur.

6. At PT of progressive metamorphism, the permeability values were high enough to permit the fluid flow to penetrate the whole volume of rock massif. At PT of regressive metamorphism, the permeability values were a few decimal orders lower, so fluid flow could be concentrated in large fracture zones only.

Acknowledgements

We appreciate the help of Dr. Yu. Smirnov, Dr. N. Galdin and Dr. K. Lobanov for providing the samples for our experiments. This work is carried out in the framework of IGCP 408 project and is supported by the Russian Foundation for Basic Researches grants:

02-05-64906, 01-05-64142, 01-05-64531 and 03-05-64153.

References

Birch, F., 1961. The velocity of compressional waves in rocks to 10 kilobars, Part 2. J. Geophys. Res. 66, 2199–2224.

Brace, W.F., 1980. Permeability of crystalline and argillaceous rocks. Int. J. Rock Mech. Min. Sci. 17, 241–251.

Chida, T., Tanaka, S., 1983. Analysis of relation between pore structure and permeability using a network model. J. Jpn. Assoc. Pet. Technol. 48 (6), 439–444.

Dodrynin, V.M., 1970. Deformations and Variations of Physical Properties of Oil and Gas Reservoir Rocks. Nedra, Moscow. 239 pp. (in Russian).

Emmerman, R., 1990. Introduction. KTB report 90-8. In: Emmerman, R., Deitrich, H.-G., Lauterjung, J., Wohrl, Th. (Eds.), KTB Pilot Hole, Results of Geoscientific Investigation in the KTB Field Laboratory, 0–4000 m, pp. b4–b8.

Gorbatzevich, F.F., Medvedev, R.V., 1986. Mechanisms of Rocks Decompaction on their Stress Relief. Ore Geophysical Investigations at Kola Peninsula. Izdatelstvo Kolskogo Filiala AN SSSR, Apatity. 83–89 pp. (in Russian).

Huenges, E., 1993. Profile of permeability and formation pressure down to 7.2 km. In: Emmermann, R., Lauterjung, J., Umsonst, T. (Eds.), KTB Report 93-2, Contributions to the 6. Annual KTB-Colloquium Geoscientific Results, Giessen, 1–2 April, pp. 279–285.

Huenges, E., Erzinger, J., Kuck, J., Engeser, B., Kessels, W., 1997. The permeable crust: geohydraulic properties down to 9101 m depth. J. Geophys. Res. 102, 18255–18265.

Kazansky, V.I., 1988. Deep structure of the continental crust and ore-forming processes. Proceedings of the Seventh Quadrennial IAGOD Symposium, Schweizerbart, Stuttgart, Germany, pp. 69–80.

Kazansky, V.I., 1992. Deep structures and metallogeny of early proterozoic mobile belts in the light of superdeep drilling in Russia. Precambrian Res. 58, 289–303.

Kazansky, V.I., Boronikhin, V.A., Vanyushin, V.A., Glagolev, A.A., Kuznetsov, Yu.T., Lanev, V.S., Lobanov, K.V., Prokhorov, K.V., Smimov, Yu.P., Starostin, V.I., 1985. Relationship between deformation, metamorphism and petrophysical properties of rocks in the Pechenga Ore District. Internal Structure of Ore-Bearing Precambrian Faults. Nauka, Moscow, pp. 6–47 (in Russian).

Kern, H., Schmidt, R., Popp, T., 1991. The velocity and density structure of the 4000 m crustal segment at the KTB drilling site and their relationship to the lithological and micro-structural characteristics of the rocks: an experimental approach. Sci. Drill. 2, 130–145.

Kern, H., Popp, T., Gorbatsevich, F., Zharikov, A., Lobanov, K.V., Smirnov, Y.P., 2001. Pressure and temperature dependence of Vp and Vs in rocks from the superdeep well and from surface analogues at Kola and the nature of velocity anisotropy. Tectonophysics 338, 113–134.

Klinkenberg, L.J., 1941. The permeability of porous media to liquids and gases. Am. Pet. Inst. Drill. Productions Practice, 200–211.

Kozlovsky, Ye.A (Ed.), 1987. The Superdeep Well of the Kola Peninsula. Springer, Berlin, p. 558.

Lobanov, K.V., Kazansky, V.I., Kuznetsov, A.V., Zharikov, A.V., Nikitin, A.N., Ivankina, T.I., Zamyatina, N.V., 2002. Correlation of archean rocks from the kola superdeep borehole and their analogues from the surface: evidence from structural–petrological, petrophysical, and neutron diffraction data. Petrology 10 (1), 23–38.

Morrow, C., Lockner, D., Hickman, S., Rusanov, M., Rockel, T., 1994. Effects of lithology and depth on permeability of core samples from the Kola and KTB boreholes. J. Geophys. Res. 99, 7263–7274.

Nikitin, A.N., Ivankina, T.I., Ullemeyer, K., Locajicek, T., Pros, Z., Klima, K., Smirnov, Yu.P., Kusnetzov, Yu.I., 2001. Texture controlled elastic anisotropy of amphibolites from the Kola superdeep borehole SG-3 at high pressure. Izvestiya, Phys. Solid Earth (English Translation of Fizika Zemli) 37, 37–45.

Shmonov, V.M., Vitovtova, V.M., Zharikov, A.V., 1995. Experimental and theoretical determination of the formation conditions for cracked fluid conducting systems under shock decompression. Exp. Geosci. 4, 56–57.

Volarovich, M.P. (Ed.), 1988. Physical properties of minerals and rocks at high thermodynamic parameters. Handbook, 2nd ed. Nedra, Moscow, p. 255 (in Russian).

Wolter, K.E., Berckhemer, H., 1989. Time dependent strain recovery of cores from KTB-deep bore hole. Rock Mech. Rock Eng. 22, 273–287.

Zharikov, A.V., Vitovtova, V.M., Shmonov, V.M., 1990. Experimental investigation of permeability of Archaean rocks from the Kola superdeep borehole. Geol. Rudn. Mestorozd. (Geology of Ore Deposits) (6), 79–88 (in Russian).